25

Modeling and Simulation of Piezoelectric Devices

Dorina Popovici, Florin Constantinescu, Mihai Maricaru,
Florea Ioan Hantila, Miruna Nitescu and Alexandru Gheorghe
Politehnica University of Bucharest
Romania

1. Introduction

The piezoelectric effect occurs in materials for which an externally applied elastic strain causes a change in electric polarization which produces a charge and a voltage across the material. The converse piezoelectric effect is produced by an externally applied electric field, which changes the electric polarization, which in turn produces an elastic strain.
The most known piezoelectric material is quartz crystal. Many other natural crystalline solids, as Rochelle salt, ammonium dihydrogen phosphate, lithium sulfate, and tourmaline as well as some man-made crystal as gallium orthophosphate, aluminium nitride (AlN), and langasite exhibit piezoelectric properties. A lot of artificial ceramics as barium titanate, lead titanate, lead zirconate titanate (PZT), potassium niobate, lithium niobate, and lithium tantalite have similar properties.
The most known technical application is the piezoelectric transducer. In the last years electromechanical AlN resonators emerged as a very efficient solution for mobile communications filters due to the possibility to be integrated at a relatively low cost together with CMOS circuits in systems on a chip and systems in a package.
In most applications the piezoelectric devices have a linear behaviour. In Section 2 the linear and nonlinear equations of the piezoelectric effect are described, a new iterative procedure for solving the nonlinear equations is given, and some aspects of the Finite Element solution are discussed. An electromechanical field analysis of a displacement transducer is presented in Section 3. Sections 4 and 5 show some recent applications in the mobile communication technology. The field analysis of a bulk acoustic wave (BAW) resonator using 3D linear models is presented in Section 4. Some nonlinear effects in power BAW resonators together with their circuit models are discussed in Section 5.

2. Electromechanical field equations of piezoelectric devices

2.1 Linear behaviour

In the case of linear behaviour (Cady, 1964; Wilson, 1989), the equations giving the

displacement **u**, the stress $\overline{\overline{t}}$ and the electric potential V are[1]:

$$\nabla \cdot \overline{\overline{t}} - \mathbf{f}_f - \rho \ddot{\mathbf{u}} = \mathbf{f} \tag{1}$$

$$-\nabla \cdot \overline{\overline{\varepsilon}} \nabla V + \nabla \cdot \mathbf{P}_M = 0 \tag{2}$$

where:

- $\overline{\overline{\varepsilon}}$ is the dielectric permittivity tensor.
- **f** is the external force.

The friction force is:

$$\mathbf{f}_f = \eta \dot{\mathbf{u}} \tag{3}$$

- The stress tensor $\overline{\overline{t}}$ has two components: $\overline{\overline{t}} = \overline{\overline{t}}_M + \overline{\overline{t}}_E$
- The mechanical stress tensor depends on the strain tensor $\overline{\overline{s}}$:

$$\overline{\overline{t}}_M = \hat{c}(\nabla_s \mathbf{u}) = \hat{c}\overline{\overline{s}} \tag{4}$$

where $\hat{c}$ is the elastic stiffness matrix evaluated for constant electric field intensity, **E=** $-\nabla V$ and $\nabla_s \mathbf{u} = \frac{1}{2}\left[(\nabla \mathbf{u}) + (\nabla \mathbf{u})^T\right]$ (the superscript T denotes the transpose of the matrix).

- The piezoelectric stress tensor depends on the electric field intensity:

$$\overline{\overline{t}}_E = \hat{e}^T(\nabla V) \tag{5}$$

where $\hat{e}$ is the piezoelectric matrix.

- The component of the polarization due to the strain is:

$$\mathbf{P}_M = \hat{e}\overline{\overline{s}} = \hat{e}(\nabla_s \mathbf{u}) \tag{6}$$

Using (3),(4),(5),(6), equations (1) and (2) become:

$$\nabla \cdot \hat{c}(\nabla_s \mathbf{u}) + \nabla \cdot \hat{e}^T(\nabla V) - \eta \dot{\mathbf{u}} - \rho \ddot{\mathbf{u}} = \mathbf{f} \tag{7}$$

$$\nabla \cdot \varepsilon \nabla V - \nabla \cdot \hat{e}(\nabla_s \mathbf{u}) = 0 \tag{8}$$

For equations (2) and (8) we consider the static regime of the electric field. In order to have a unique solution, mechanical and electrical boundary conditions must be added: $\mathbf{u} = 0$, for clamped surfaces, $\mathbf{n}\overline{\overline{t}} = 0$, for free surfaces, a hybrid boundary condition (BC) in the case of a very light movable electrode; V = imposed for electrodes, $\mathbf{n} \cdot \mathbf{D} = 0$ for field surfaces or symmetry surfaces, where:

$$\mathbf{D} = -\overline{\overline{\varepsilon}} \nabla V + \mathbf{P}_M \tag{9}$$

[1] *Notations*: the boldface letters represent vectors, tensors are represented as $\overline{\overline{t}}$, $\nabla \mathbf{u}$ is a diadic product, while $\nabla \cdot \mathbf{u}$ is a scalar product and a dot above a variable denotes a time derivative..

The friction forces are neglected for modal analysis. Equations (7) and (8) become:

$$\nabla \cdot \hat{c}(\nabla_s \mathbf{u}) + \nabla \cdot \hat{e}^T(\nabla V) + \omega^2 \rho \mathbf{u} = \mathbf{0} \tag{10}$$

$$\nabla \cdot \varepsilon \nabla V - \nabla \cdot \hat{e}(\nabla_s \mathbf{u}) = 0 \tag{11}$$

The values ω_k which allow nontrivial solutions $\mathbf{u}_k$ of equations (10),(11) give resonance frequencies.

2.2 Nonlinear constitutive equations

The nonlinear behaviour can be modelled using the nonlinear constitutive equations:

1. The friction force depends nonlinearly on the velocity (time derivative of displacement):

$$\mathbf{f}_f = F(\dot{\mathbf{u}}) \tag{12}$$

2. The relationship $\bar{\bar{t}} - \bar{\bar{s}}$ is nonlinear. This is possible in the case of large strains (powerful stress). The dielectric may be destroyed and the durability decreases. Hence, this case must be avoided.
3. The relationship **D-E** is nonlinear:

$$\mathbf{D} = \mathsf{D}(-\nabla V) + \mathbf{P}_M \tag{13}$$

We do not know yet results which present this kind of relationship.

4. The relationships of the piezoelectric effects are nonlinear:

$$\bar{\bar{t}} = \mathsf{T}(\mathbf{E}) \tag{14}$$

$$\mathbf{P}_M = \mathsf{P}(\bar{\bar{s}}) \tag{15}$$

If the complementary energy may be defined:

$$\delta U^* = \sum_{i,j=1}^{3} t_{ij} ds_{ij} - \sum_{k=1}^{3} P_k dE_k \tag{16}$$

we have:

$$\frac{\partial \mathsf{T}_{ij}}{\partial E_k} = -\frac{\partial \mathsf{P}_k}{\partial s_{ij}} \tag{17}$$

In the linear case, relationship (17) defines the same matrix $\hat{e}$ in (5) and (6).

2.3 Iterative Procedures for Nonlinear Materials

The usual method taking into account the nonlinearity is Newton-Raphson, which is used in most commercial simulators. This method provides a great convergence speed, but in some cases the convergence is not always achieved.

The nonlinearity of the friction force relationship may be treated using the fixed point Picard-Banach procedure. We replace the relation (12) by:

$$\mathbf{f}_f = \eta\dot{\mathbf{u}} + \mathbf{f}_r \tag{18}$$

where the nonlinearity is contained in:

$$\mathbf{f}_r = F(\dot{\mathbf{u}}) - \eta\dot{\mathbf{u}} = G(\dot{\mathbf{u}}) \tag{19}$$

It may be proved (Hantila et al., 2000) that if the function F is uniformly monotonic

$$\big(F(\mathbf{a}) - F(\mathbf{b})\big)\cdot(\mathbf{a}-\mathbf{b}) \geq \lambda|\mathbf{a}-\mathbf{b}|^2\ ,\ \lambda > 0\ ,\ \ \forall \mathbf{a},\mathbf{b} \tag{20}$$

and Lipschitzian

$$\big|F(\mathbf{a}) - F(\mathbf{b})\big| < \Lambda|\mathbf{a}-\mathbf{b}|\ ,\ \ \forall \mathbf{a},\mathbf{b} \tag{21}$$

we can find a value for η so that the function G, defined by (19) is a contraction i.e.

$$\big|G(\mathbf{a}) - G(\mathbf{b})\big| \leq \theta|\mathbf{a}-\mathbf{b}|\ ,\ \ \theta < 1\ ,\ \ \forall \mathbf{a},\mathbf{b} \tag{22}$$

We propose the following iterative procedure:

a. We choose an arbitrary initial value $\mathbf{f}_r^{(0)}$.
b. We compute $\mathbf{u}^{(1)}$ and hence $\dot{\mathbf{u}}^{(1)}$ solving the system (7) and (8), where the force $\mathbf{f}$ is replaced by $\mathbf{f} + \mathbf{f}_r^{(0)}$.
c. We correct the force $\mathbf{f}_r$ with (19):

$$f_r^{(1)} = G(\dot{\mathbf{u}}^{(1)}) \tag{23}$$

The steps b) and c) are repeated until the error

$$er^{(n)} = \int_{\Omega}\int_0^t \eta\left(\Delta\dot{\mathbf{u}}^{(n)}\right)^2 d\tau d\Omega = \left\|\Delta\dot{\mathbf{u}}^{(n)}\right\|_\eta^2 \tag{24}$$

is small enough, where $\Delta\dot{\mathbf{u}}^{(n)} = \dot{\mathbf{u}}^{(n)} - \dot{\mathbf{u}}^{(n-1)}$.
It may be proved that for a given $\mathbf{f}_r$ equations (7) and (8) have a unique solution $\mathbf{u}$, hence $\dot{\mathbf{u}} = W(\mathbf{f}_r)$ and the function W is non-expansive:

$$\big|W(\mathbf{a}) - W(\mathbf{b})\big| \leq |\mathbf{a}-\mathbf{b}|\ ,\ \ \forall \mathbf{a},\mathbf{b} \tag{25}$$

Therefore, the above procedure gives the Picard-Banach convergent sequence of the contraction $\mathsf{G}W$, where the function $\mathsf{G}: L^2([0,t]\times\Omega) \to L^2([0,t]\times\Omega)$ is defined by the local function G. The procedure has several important advantages: we may evaluate the errors with respect to the exact solution, the overrelaxation may be applied, the system matrix of the numerical form of equations (7), (8) is the same at each iteration.
The most convenient procedure for space discretization of equations (7), (8) is the finite element method (see (Makkonen et al., 2001), for instance). The spectral decomposition is recommended for time discretization.

2.4 FEM solution of the coupled electromechanical field problem

In Finite Element Method (FEM), the complete problem domain is discretized. This implies that FEM encounters inherent difficulties in dealing with open boundary field problems, as the problem domain needs to be truncated to keep the size finite. Truncation inevitably introduces an artificial boundary and, consequently, a modelling error resulting from an approximation of the BC on this boundary. Considering acoustic waves, the truncation of the model causes reflections of the wave on the artificial boundaries (see Fig. 1).

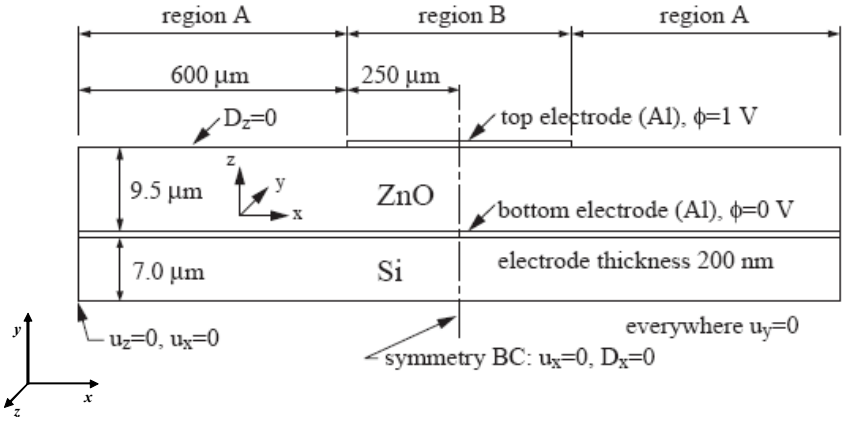

Figure 1. Cross section of a membrane-type composite thin-film BAW resonator showing the boundary conditions imposed in the FEM model

Placing infinite elements along the artificial boundary on the side of the continuum has been suggested as a solution to this problem. The infinite elements strive to implement an ideal absorbing boundary condition, such that a wave incident on the boundary would not reflect back. Instead of infinite elements, one may simply introduce regions at the boundaries of the model where the attenuation of the material increases from zero to a given finite value. Since the increase of the attenuation is gradual, there is no abrupt change in the materials properties which would give rise to reflections of the wave. With a sufficiently high attenuation, the amplitude of the wave entering the region will decay rapidly such that there is no reflection. This solution has the benefit that it can be readily applied without any need for special FEM elements (Makkonen, 2005).

A possible solution is to combine FEM with another method which is used to model the semi-infinite region. An example of such a modelling technique is the FEM/boundary-element-method (BEM) formalism, which is used in the modelling of surface-acoustic wave devices.

The electromechanical constitutive equations for linear material behaviour that FEM softwares solve are:

$$\begin{aligned} \mathbf{T} &= c_E \mathbf{S} - e\mathbf{E} \\ \mathbf{D} &= e^T \mathbf{S} + \varepsilon_S \mathbf{E} \end{aligned} \tag{26}$$

where: **T** is the stress vector (referred to as σ elsewhere); **D** is the electric flux density vector; **S** is the strain vector (referred to as ε elsewhere); **E** is the electric field vector; c_E is the

elasticity matrix (evaluated at constant electric field); e is piezoelectric stress matrix, and ε_S is the dielectric matrix (evaluated at constant mechanical strain).
The elasticity matrix c can be given directly in uninverted form [c] as a general anisotropic symmetric matrix:

$$c_E = \begin{bmatrix} c_{11} & c_{12} & c_{13} & c_{14} & c_{15} & c_{16} \\ & c_{22} & c_{23} & c_{24} & c_{25} & c_{26} \\ & & c_{33} & c_{34} & c_{35} & c_{36} \\ & & & c_{44} & c_{45} & c_{46} \\ & \text{symmetric} & & & c_{55} & c_{56} \\ & & & & & c_{66} \end{bmatrix} \tag{27}$$

The input can also be c_D, the elasticity matrix (evaluated at constant electric flux density):

$$c_D = c_E + \frac{e^2}{\varepsilon_S} \tag{28}$$

The piezoelectric stress matrix e relates the electric field vector **E** in the order *x, y, z* to the stress vector **T** in the order *x, y, z, xy, yz, xz* and has the form:

$$e = \begin{bmatrix} e_{11} & e_{12} & e_{13} \\ e_{21} & e_{22} & e_{23} \\ e_{31} & e_{32} & e_{33} \\ e_{41} & e_{42} & e_{43} \\ e_{51} & e_{52} & e_{53} \\ e_{61} & e_{62} & e_{63} \end{bmatrix} \tag{29}$$

The piezoelectric matrix can also be given as a piezoelectric strain matrix d. The piezoelectric strain matrix d can be converted to the piezoelectric stress matrix e using the elasticity matrix c:

$$e = c \cdot d \tag{30}$$

The dielectric matrix ε_S uses the electrical permittivities and can be described in orthotropic or anisotropic form:

$$\varepsilon_S = \begin{bmatrix} \varepsilon_{11} & 0 & 0 \\ 0 & \varepsilon_{22} & 0 \\ 0 & 0 & \varepsilon_{33} \end{bmatrix} \text{ or } \varepsilon_S = \begin{bmatrix} \varepsilon_{11} & \varepsilon_{12} & \varepsilon_{13} \\ & \varepsilon_{22} & \varepsilon_{23} \\ symmetric & & \varepsilon_{33} \end{bmatrix} \tag{31}$$

The dielectric matrix can also be given as a dielectric permittivity matrix at constant stress ε_T. We can convert the dielectric matrix at constant stress to the dielectric matrix at constant strain:

$$\varepsilon_S = \varepsilon_T - e^T d \tag{32}$$

The finite element discretization is performed by establishing nodal solution variables and element shape functions over an element domain which approximates the solution.

$$u_c = N_u^T \cdot u \tag{33}$$

$$V_c = N_V \cdot V \tag{34}$$

where: u_c is the displacement within element domain in the x, y, z directions; V_c is the electrical potential within element domain; N_u is the matrix of displacement shape functions; N_V is the vector of electrical potential shape function; u is the vector of nodal displacements, and V is the vector of nodal electrical potential.
Then the strain **S** and electric field **E** are related to the displacements and potentials, respectively, as:

$$\mathbf{S} = B_u \cdot u \tag{35}$$

$$\mathbf{E} = -B_V \cdot V \tag{36}$$

$$B_u = \begin{bmatrix} \frac{\partial}{\partial x} & 0 & 0 & \frac{\partial}{\partial y} & 0 & \frac{\partial}{\partial z} \\ 0 & \frac{\partial}{\partial y} & 0 & \frac{\partial}{\partial x} & \frac{\partial}{\partial z} & 0 \\ 0 & 0 & \frac{\partial}{\partial z} & 0 & \frac{\partial}{\partial y} & \frac{\partial}{\partial x} \end{bmatrix}^T \tag{37}$$

$$B_V = \begin{bmatrix} \frac{\partial}{\partial x} & \frac{\partial}{\partial y} & \frac{\partial}{\partial z} \end{bmatrix}^T \tag{38}$$

After the application of the variational principle and finite element discretization, the coupled finite element matrix equation is:

$$\begin{bmatrix} M & 0 \\ 0 & 0 \end{bmatrix} \begin{bmatrix} \ddot{u} \\ \ddot{V} \end{bmatrix} + \begin{bmatrix} C & 0 \\ 0 & 0 \end{bmatrix} \begin{bmatrix} \dot{u} \\ \dot{V} \end{bmatrix} + \begin{bmatrix} K & K_z \\ K_z^T & K_d \end{bmatrix} \begin{bmatrix} u \\ V \end{bmatrix} = \begin{bmatrix} F \\ L \end{bmatrix} \tag{39}$$

The following equations provide an explanation of the submatrices in (39).
Structural mass (ρ is the mass density):

$$M = \int_{element} \rho N_u N_u^T dv \tag{40}$$

The damping matrix (C) may be used in harmonic, damped modal and transient analyses as well as substructure generation. In its most general form, it is:

$$M = \alpha M + (\beta + \beta_c) K + \sum_{j=1}^{N_m} \left[\left(\beta_j^m + \frac{2}{\Omega} \beta_j^\xi \right) K_j \right] + \sum_{k=1}^{N_e} C_k + C_\xi \tag{41}$$

where: C is the structure damping matrix; a is the mass matrix multiplier; M is the structure mass matrix; β is the stiffness matrix multiplier; β_c is the variable stiffness matrix multiplier; K is the structure stiffness matrix; N_m is the number of materials with β_j^m (stiffness matrix multiplier for material j), β_j^{ξ} (constant (frequency-independent) stiffness matrix coefficient for material j, Ω - circular excitation frequency) and K_j the portion of structure stiffness matrix based on material j; N_e is the number of elements with specified damping (C_k - element damping matrix, C_ξ - frequency-dependent damping matrix).
Structural stiffness:

$$K = \int_{element} B_u^T c B_u dv \tag{42}$$

Dielectric conductivity:

$$K_d = - \int_{element} B_V^T \varepsilon B_V dv \tag{43}$$

Piezoelectric coupling matrix:

$$K_z = - \int_{element} B_u^T e B_V dv \tag{44}$$

Structural load vector, F, is a vector of nodal forces, surface forces, and body forces. Electrical load vector, L, is a vector of nodal, surface, and body charges.
In a FEM mesh, each node point is connected only to a limited number of other nearby located nodes. The benefit of this local connectivity is that the FEM matrices (system matrices) which describe the complete modelled system have a band structure. The relevant system matrices are the electromechanical stiffness matrix K and mass matrix M. In each node point of the FEM mesh, at least four field variables are considered (i.e., the three components of displacement and the electric potential). The values of the fields at a node point are the unknowns or degrees of freedom (DOFs) which are finally computed from the FEM equations.
In the modal analysis, the eigenproblem resulting from the FEM formulation is solved for the frequencies of the vibration modes (eigenfrequencies) and for their mode shapes (eigenvectors).
FEM software can also solve the field problem, where the response of the structure to time harmonic loading is computed. In harmonic analysis, the damping can be taken into account, since a solver for complex-valued linear systems of equations can be included into the FEM software.
Starting from coupled electroelastic equations (Ostergaard & Pawlak, 1986) four types of solutions are possible:

- Static Analysis (inertial and damping effects are ignored except static acceleration effects such as gravity; displacements and/or electric potentials are obtained).
- Mode-Frequency Analysis (mode shapes and natural frequencies may be obtained).
- Harmonic Analysis (the investigation of a piezoelectric structure under the influence of harmonic forces, currents, displacements, and/or voltages; system response characteristics to harmonic loads are obtained).

- Transient Analysis (the investigation of a piezoelectric structure under the influence of time-dependent forces, currents, displacements, and/or voltages; transient response of the system is computed).

3. Field analysis of a displacement transducer

The FEM analysis of a cantilever beam deformation producing electrical voltages trough a direct piezoelectric effect is described in the following (Dorina Popovici et al., 2006).

3.1 Geometry of the model

To simulate the structure we have chosen a multiphysics problem: plane stress and piezo plane stress. The geometry used is presented in figure below:

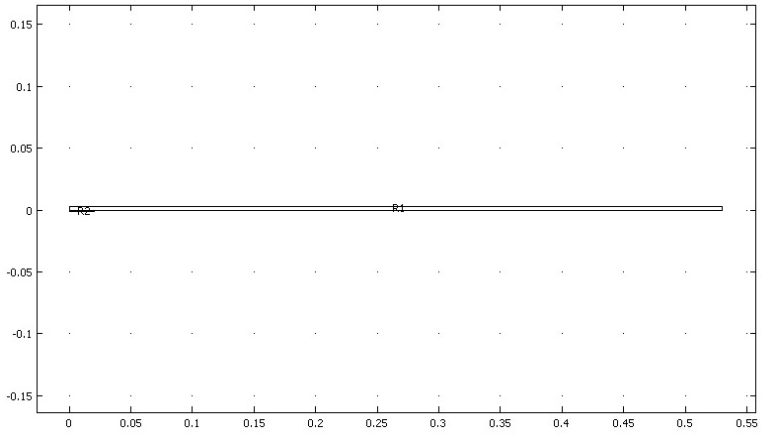

Figure 2. The geometry of the problem

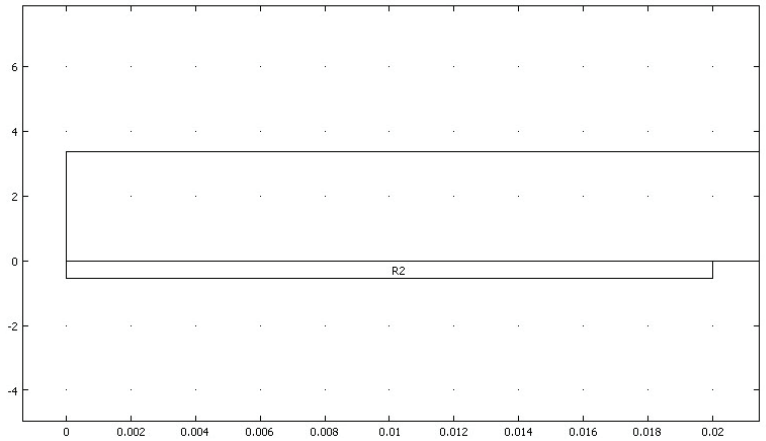

Figure 3. Zoom in the PZT cell section

The domain R1 is an isotropic structural steel beam with a length of 550 mm, width of 50 mm and thickness of 5 mm. This material is defined in Library 1 of (COMSOL, 2005). The domain R2 is the PZT 5H cell which has a length of 20 mm, width of 50 mm and thickness of 0,5 mm.

For the structural steel we used the following material constants E = $2 \cdot 10^5$ [MPa], Poisson's ratio ν = 0.33 and density ρ = 7850 kg/m^3.

The PZT – 5H properties are those listed in (COMSOL, 2005): c_E (c_{11}=c_{22}=126, c_{12}=80.5, c_{13}=c_{23}=126, c_{33}=117, c_{44}=23.3, c_{55}=c_{66}=23, all in GPa), e(e_{51}= e_{42}=17, e_{13}= e_{23}=17, e_{33}= 23.3, [C/m^2]), ε_S (ε_{11} = ε_{22} =1704, ε_{33} =1433, relative values).

The boundary conditions resulted from the working conditions. For the mechanical part of the problem a constraint of zero displacement on the left side of the beam and the PZT cell has been considered. The load was applied on the right end of the beam only on the y direction.

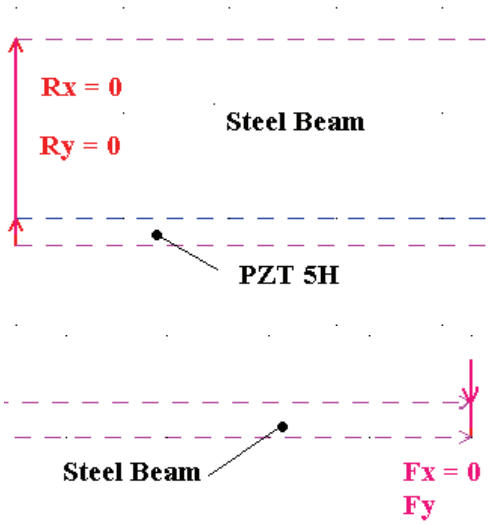

Figure 4. The mechanical boundary conditions

We set the horizontal bottom surface of the PZT cell to ground and a zero charge/symmetry condition was considered on the top surface.

The meshed model contains 3516 triangular elements.

3.2 Results

Three basic analysis types available in the Structural Mechanics Module have been considered:

- Static
- Eigenfrequency
- Transient.

At first, a statical analysis has been made, where a uniform distributed load has been applied at the right end of the beam. This force has only a vertical component f_y = 10000

N/m. The stationary direct linear solver UMFPACK has been used. In Fig. 5, 6, 7 are represented the displacements along the y axis, the maximum displacement at the end of the beam, and the local voltage along the PZT cell.

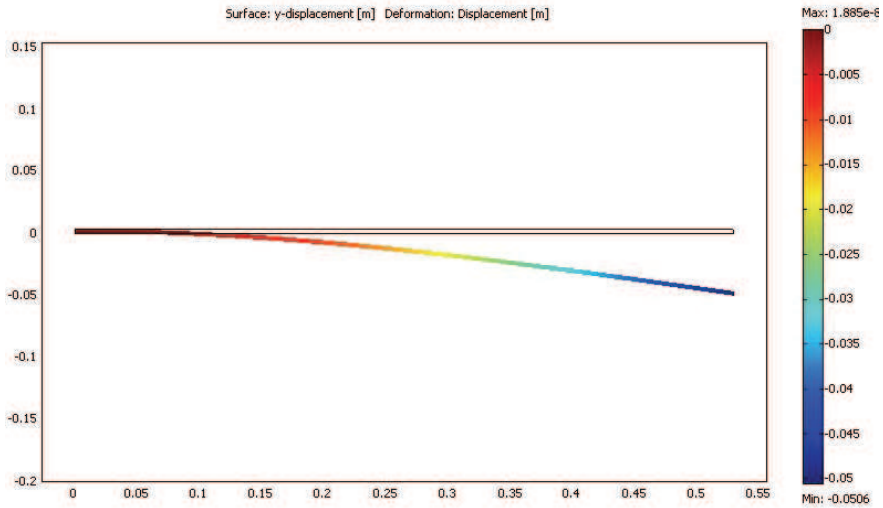

Figure 5. Displacement of the beam on the y axis for f_y = 10000 [N/m]

The maximum stress calculated with Von Mises criteria has been determined in the left side of the beam (in the vicinity of the clamping side) and was equal to 294 [MPa] and the minimum value in the right side of the beam 0,168 [MPa].

The voltage response of the PZT cell at different loads ($f_y \in$ {500, 1000, 2500, 5000, 7500, 10000} [N/m]) has a linear variation as we can see in Fig. 8. For the same loads we determined the displacement on y axis of the right side of the beam (Fig. 9) and the maximum stress values (Fig. 10) which has the same linear variation.

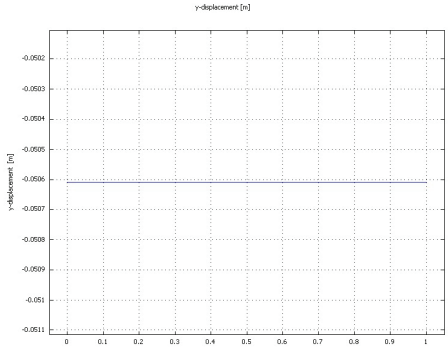

Figure 6. y -displacement of the right end of the beam vs. relative position on z

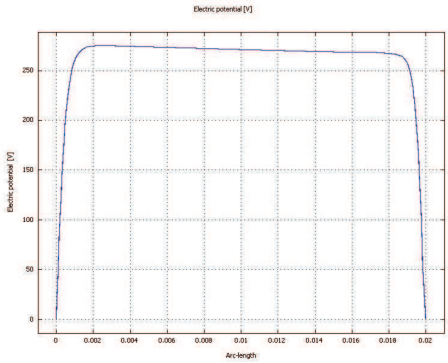

Figure 7. Local voltage vs. longitudinal position along PZT cell

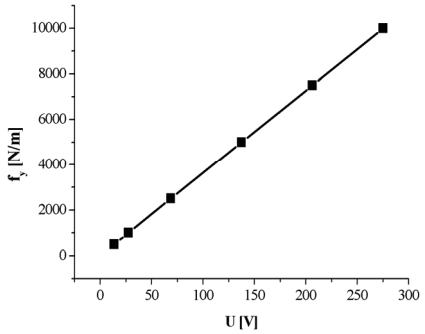

Figure 8. The linear dependence F(U)

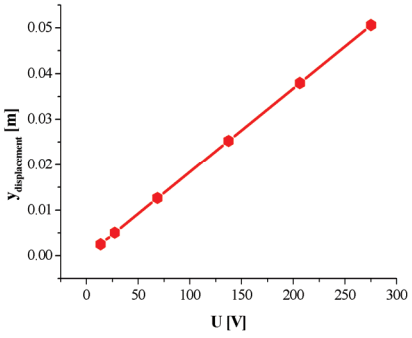

Figure 9. Displacement of the right end of the beam

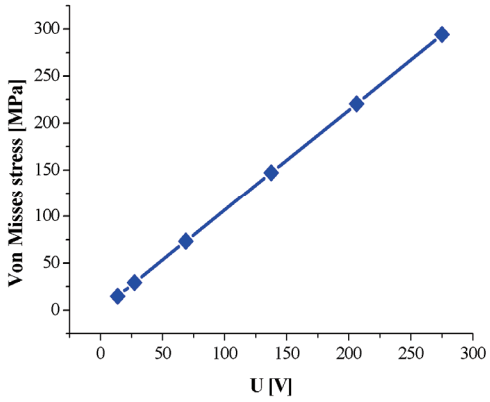

Figure 10. The maximum stress values

The simulation results used to draw figures 8 to 10 are given in Table 1.

f_y [N/m]	Von Misses stress [MPa]	$y_{displacement}$ [mm]	U [V]
500	14.71	2.53	13.75
1000	29.42	5.06	27.51
2500	73.55	12.65	68.77
5000	147.1	25.30	137.55
7500	220.6	37.95	206.33
10000	294.2	50.61	275.10

Table 1. Values determined in statical analysis

An eigenfrequency analysis finds the eigenfrequencies and modes of deformation of the analyzed structure. The eigenfrequencies `f` in the structural mechanics field are related to the eigenvalues λ returned by the solvers through:

$$f = \frac{\sqrt{\lambda}}{2\pi}$$

The purpose of the eigenfrequency analysis is to find the six lowest eigenfrequencies and their corresponding shape modes. This model uses the same material, load and constraints as the statical analysis. A direct system solver Umfpack was used and the results are presented below:

f_1	f_2	f_3	f_4	f_5	f_6
9.98 Hz	64.48 Hz	174.73 Hz	341.91 Hz	564.31 Hz	841.75 Hz

Table 2. The first six eigenfrequencies of the model

A transient analysis giving the displacements and velocities as functions of time was used. In this case, loads and boundary conditions are functions of time. The purpose of this analysis was to find the transient response to a harmonic load with the same amplitude as the static load during the first two periods. The excitation frequency has been taken 50 Hz,

which is between the first and second eigenfrequency found in the eigenfrequencies analysis.

A harmonic load $f_x = 0$ and $f_y = 10000 \sin(100\,\pi\, t)$ [N/m] has been used. Damping is very important in transient analysis but difficult to model. The Structural Mechanics Module supports Rayleigh damping, specifying damping parameters proportional to the mass (α_{dM}) and stiffness (β_{dK}) in the following way:

$$C = \alpha_{dM} M + \beta_{dK} K$$

where `C` is the damping matrix, `M` is the mass matrix, and `K` is the stiffness matrix. The structure has a constant damping ratio of 0.1. Two frequencies near the excitation frequency (20Hz and 60 Hz) have been considered to calculate the damping parameters, according to the FEMLAB code (COMSOL, 2005): $\alpha_{dM} = 18.849$ 1/s and $\beta_{dK} = 3.979 \cdot 10^{-4}$ s.

The computation used a solver with the time interval [0; 0.08][s] within a step of 0.001, a relative tolerance of 0.05 and an absolute tolerance of 10^{-9}.

The following waveforms for the displacement on the x and y axes are represented in Fig.11 and 12.

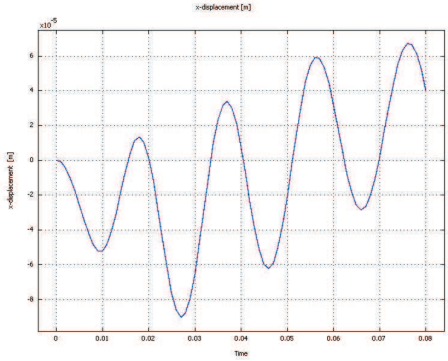

Figure 11. The x displacement of the right end of the beam

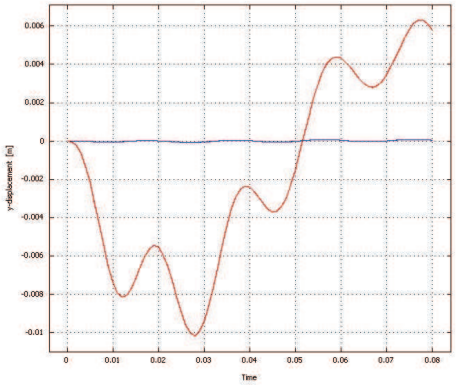

Figure 12. The x displacement (__) and the y displacement (__) of the right end of the beam

The voltage output computed on the PZT crystal has a sinusoidal figure with a maximum value of 182.072 [V] and a minimum value of -150.962 V.

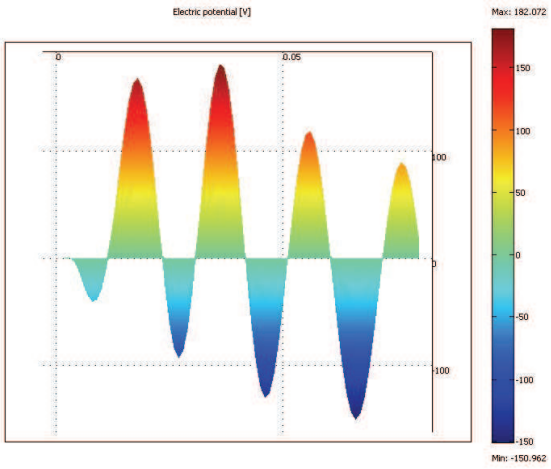

Figure 13. The PZT crystal voltage vs. time

For a more accurate solution the time interval has been increased from 0.08 to 0.2 [s] ; in this case, the total displacement and the equivalent voltage response are represented in Fig.14 and 15.

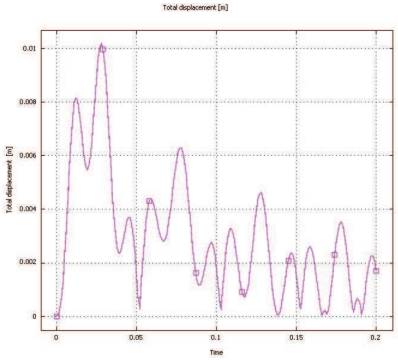

Figure 14. The total displacement of the right side of the beam

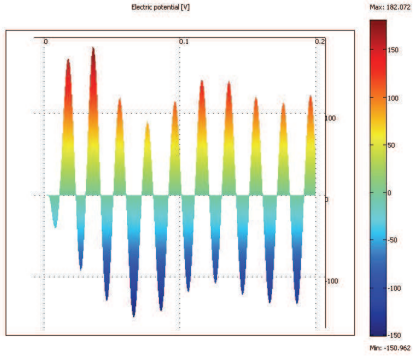

Figure 15. The PZT crystal voltage

4. Field analysis of a BAW resonator

We assume that the cause for material deterioration is the high level of the local stress in resonator layers. It follows that the regions in which material deteriorates correspond to the regions of maximum local stress.
To compute the local stress FEM analysis of a 3D electromechanical field problem must be done. In order to do this, material parameters of various resonator layers must be known. A part of them haven't been measured directly for the case in point, being taken from literature. To verify the parameter values, a model taking into account only longitudinal wave propagation (on z axis) has been analyzed, the results being reported in paragraph 4.1. Further on, a 3D model of a quarter of a resonator is analyzed in paragraph 4.2.
For piezoelectric analysis (ANSYS, 2005) performs the so called "strong coupling analysis" meaning that the whole equation system of the coupled field problem is used.

4.1 Numerical simulation of longitudinal wave propagation in a BAW resonator structure

Mat. No.	Material	Density ρ [kg/m^3]	Longitudinal velocity [m/s]	c_{33} [GPa]	ε_{33} [pF/m]	e_{33} [C/m^2]
1	Mo	10000	6600	435.6		
3	SiOC	1500	2400	10.14		
4	SiN	2700	9300	233.523		
5	Si	2330	8400	164.4		
6	AlN	3300	11000	399.3	82.6	1.5

Table 3. Material properties used for analytical model simulations

Block No.	Mat. No.	Material
1	4	SiN
3	1	Mo
4	6	AlN
5	1	Mo
6	3	SiOC
7	4	SiN
8	3	SiOC
9	4	SiN
10	3	SiOC
11	5	Si substrate

Table 4. List of materials used to fabricate the device

Additional material properties:
AlN c11=345 GPa, c12=125 GPa, c13=120 GPa, c22= 345 GPa, c23= 120 GPa, c33= 372.06 GPa, c44= 118 GPa, c55= 110 GPa, c66= 110 GPa (each at constant E field) e33= 1.5 C/m², e13= -0.58 C/m², e23=-0.58 C/m²
Si Major Poisson's ratios: PRXY=PRYZ=PRXZ=0.26, Young's Modulus Ex=Ey=Ez= 134.36 GPa
SiN PRXY=PRYZ=PRXZ=0.29, Ex=Ey=Ez= 178.20 GPa
SiOC PRXY=PRYZ=PRXZ=0.22, Ex=Ey=Ez= 8.88 GPa
Mo PRXY=PRYZ=PRXZ=0.31, Ex=Ey=Ez= 314.26 GPa

The resonator has an area of 22500 μm².
Other assumptions about the model:
Mechanical boundary conditions: zero displacement constraints for all directions imposed on the bottom surface of the last block (only for stack configuration 10).
Meshing:

- Only one 3-D 20-node brick element is considered in all transversal sections (the transversal waves of propagation are practically neglected).
- Each layer is meshed longitudinally with a number of 3-D 20-node brick elements, that have the height less than 1/8 of the wavelength, and this number is increased until we reach the stability of the resonance and antiresonance frequency values.

This stable solution is reached in general for elements with heights about 1/(16÷25) of the wavelength.
Mechanical losses have been taken into account by using a constant damping ratio of $3x10^{-3}$.
In this model only longitudinal wave propagation is reproduced. The FEM analysis results have been computed adding layer by layer and are given in the following. The resonance frequencies are compared to those obtained using the Mason multilayer model.

Stack configuration	**Resonance frequencies computed with FEM simulation**	**FEM simulation result**
Config 1: only AlN 1170 nm	*Fr* = 4.568 GHz, *Fa* = 4.702 GHz Mason model: $F_a = \frac{1}{2l}\sqrt{\frac{c_{33}+\frac{e_{33}^2}{\varepsilon_{33}}}{\rho}} = 4.7009\,\text{GHz}$ (simple anti-resonance formula for thickness mode)